Paper I

Tore Birkeland, Morten Førre, Jan Petter Hansen and Sølve Selstø

Dynamics of H(2p) ionization in ultrashort strong laser pulses

Journal of Physics B **37**, 4205 (2004).

INSTITUTE OF PHYSICS PUBLISHING JOURNAL OF PHYSICS B: ATOMIC, MOLECULAR AND OPTICAL PHYSICS

J. Phys. B: At. Mol. Opt. Phys. **37** (2004) 4205–4219 PII: S0953-4075(04)84345-1

Dynamics of H(2p) ionization in ultrashort strong laser pulses

T Birkeland, M Førre, J P Hansen and S Selstø

Department of Physics and Technology, University of Bergen, N-5007 Bergen, Norway

Received 27 July 2004
Published 12 October 2004
Online at stacks.iop.org/JPhysB/37/4205
doi:10.1088/0953-4075/37/20/014

Abstract

The ionization dynamics of an initially excited aligned H(2p, $m = 0$) atom exposed to short intense laser pulses is studied in the non-perturbative regime based on a three-dimensional numerical solution of the time-dependent Schrödinger equation on a spherical grid. The laser pulse is given a linear polarization vector which defines an angle θ with the symmetry axis of the initial 2p state. Strong orientation effects for ionization are found as a function of polarization direction for high laser frequencies. The angular distribution of the photo-electron spectrum shows two characteristic features related to ionization dynamics and interference of parallel versus perpendicular states with respect to the polarization direction of the field. For high enough field intensities, the ionization probability saturates below unity. In this limit, the angular electronic distribution is insensitive to the laser polarization direction. Another characteristic feature is a complete suppression of multiphoton peaks which results in kinetic emission spectra dominated by slow electrons.

(Some figures in this article are in colour only in the electronic version)

1. Introduction

In recent years, the experimental tools to study dynamical processes of atom and molecule interactions with electromagnetic fields have improved dramatically. For example, attosecond laser pulses with phase control are now realized [1] and open for imaging of ultrafast dynamics such as time-dependent Auger processes [2] or nuclear dynamics [3]. Other examples involve preparation of aligned molecules [4] and momentum recoil analysis of fragmenting products [5, 6] utilizing real studies of reaction dynamics to a degree which only a few years ago were at the 'gedanken' level.

In order to interpret and understand the basic underlying quantum mechanics, the need to solve the time-dependent Schrödinger equation in parallel with the experimental progress is strengthened [7]. This requires development and evaluation of numerical methods for

increasingly complex systems with a corresponding increasing number of degrees of freedom. For linear polarized laser light interacting with spherically symmetric ground state atoms, the symmetry reduction to two effective degrees of freedom has resulted in a variety of methods [8] which has been applied to a range of phenomena such as above threshold ionization (ATI) [9], dynamic stabilization (DS) [10] and high harmonic generation [11]. A few groups, however, have reported related studies with broken cylindrical symmetry, e.g., atomic stabilization in intense circular polarized light [12, 13] molecular dynamics [14] and interaction with excited hydrogen [15].

Analogous to such studies of light–matter interactions with circular polarized light, interactions between initially aligned atoms or molecules in general need a full three-dimensional analysis as well [16]. An example is here the ability of a diatomic molecule to ionize as a function of the angle between the (linear) laser polarization vector and the molecular internuclear axis. A strong alignment dependence on the ionization probability of diatomic molecules exposed to femtosecond laser pulses was recently experimentally demonstrated [17]. On the theoretical side, molecular alignment effects and the interplay between nuclear and electronic dynamics has only been studied within perturbation schemes [18, 19] or low-dimensional models [20, 21].

Concerning alignment and increasingly intense laser fields, it is well known that the ionization probability of ground state atoms at some point may start to decrease, or alternatively saturate at a level below 1 [10]. The geometrical aspects of this process for aligned atoms have only been briefly documented previously [15].

The present paper has two main components (i) an analysis of numerical methods and (ii) an application of the best method to calculate the ionization probability and the energy spectrum of an initially excited hydrogen atom in the 2p state with vanishing angular momentum around the quantization axis. The atom is exposed to a 5-cycle laser pulse with frequency either in the XUV region or in the UV region. The linear polarization vector defines in both cases an angle θ with the quantization axis. An extremely strong orientation effect is predicted for the XUV radiation, whereas the UV light produces a much more modest orientation effect. This is in contrast to calculations of similar orientation effects in diatomic molecules [25] and indicates that new orientation effects might be observed for diatomic Π state molecules in contrast to Σ state molecules [17].

The calculations are based on a three-dimensional spectral split step method. The method is shown to behave very efficiently in the Kramers–Henneberger frame for strong pulsed laser fields. It is based on an original two-dimensional formulation by Hermann and Fleck [22] which was recently extended to three dimensions [23]. The paper is organized as follows: in the following section, the numerical method is described. In section 3, the calculations are presented and the results are interpreted. Atomic units, $m_e = \hbar = e = 1$, are used unless otherwise stated.

2. Three-dimensional spectral method

A hydrogen atom interacting with the classical electromagnetic field is conveniently described by the semi-classical Hamiltonian,

$$H = \frac{1}{2}[\mathbf{p} + \mathbf{A}(\mathbf{r}, t)]^2 - \frac{1}{r}, \tag{1}$$

where $\mathbf{A}(\mathbf{r}, t)$ is the electromagnetic vector potential. In the present formulation we assume the dipole approximation to be valid, i.e. the wavelength of the radiation is much larger than the extent of the atom. For moderate intensity, laser frequency and pulse duration, this is

an excellent approximation. However, for the highest intensities in section 3, it has been shown that non-dipole effects start to become important [24]. When the dipole approximation applies, $\mathbf{A}(\mathbf{r}, t) \approx \mathbf{A}(t)$, and when introducing spherical coordinates the effective Hamiltonian can be expressed in the so-called *velocity gauge*,

$$H(\mathbf{r}, t) = -\frac{1}{2}\frac{\partial^2}{\partial r^2} + \frac{\mathbf{L}^2(\Omega)}{2r^2} + V_v(r, \Omega, t) = H_0 + V_v(r, \Omega, t), \tag{2}$$

with

$$V_v(r, \Omega, t) = -\frac{1}{r} + \mathbf{A}(t) \cdot \nabla. \tag{3}$$

Here $\Omega = (\theta, \phi)$ denotes the spherical angles. This Hamiltonian governs the time evolution of the reduced wavefunction $\Phi(\mathbf{r}, t) = r\Psi(\mathbf{r}, t)$. The squared term of the vector potential of equation (2) contributes in the dipole approximation to the wavefunction only as a global phase factor. This factor is routinely removed by the transformation $\Psi_v(\mathbf{r}, t) \rightarrow \Psi_v(\mathbf{r}, t)\, \mathrm{e}^{-\mathrm{i}/2 \int_0^t \mathbf{A}^2(t')\mathrm{d}t'}$. The velocity gauge is a frequently used starting point for perturbation theories [25] as well as non-perturbative treatments [26].

An alternative formulation which is explicitly based on the physical electric and/or magnetic fields is obtained by the transformation

$$\Psi_l(\mathbf{r}, t) = U_{v\rightarrow l}\Psi_v(\mathbf{r}, t) \tag{4}$$

with, $U_{v\rightarrow l} = \mathrm{e}^{-\mathrm{i}\mathbf{r}\cdot\mathbf{A}(t)}$. Since the electric field is related to the vector potential by, $\mathbf{E}(\mathbf{r}, t) = -\partial_t \mathbf{A}(\mathbf{r}, t)$, we obtain the *length gauge* Hamiltonian $H = H_0 + V_l(r, \Omega, t)$ where the potential is given by,

$$V_l(r, \Omega, t) = -\frac{1}{r} + \mathbf{E}(\mathbf{r}, t) \cdot \mathbf{r}. \tag{5}$$

Alternatively, the laser pulse may be described from the accelerated frame [27] following the motion of a free electron in the field. The frame transformation is defined by $U_{v\rightarrow a} = \mathrm{e}^{-\mathrm{i}\mathbf{p}\cdot\boldsymbol{\alpha}(t)}$ which gives the Kramers–Henneberger (KH) frame Hamiltonian, $H = H_0 + V_a(r, \Omega, t)$, with

$$V_a(r, \Omega, t) = -\frac{1}{|\mathbf{r} + \boldsymbol{\alpha}(t)|}. \tag{6}$$

The quantity $\boldsymbol{\alpha}(t)$ is the electron field displacement vector defined by $\boldsymbol{\alpha}(t) = \int_0^t \mathbf{A}(t')\,\mathrm{d}t'$. In the KH frame, the effect of the laser is thus 'seen' from the position of the electron as a nucleus oscillating with the characteristic frequency of the laser pulse. We note that the KH transformation is closely related to the electronic translational factors (ETF) applied to almost all non-perturbative two-centre descriptions of ion–atom collisions where the ETF factors not only ensure Galilean invariance of the theory, but also strongly limit the number of states needed to describe electron capture processes [28].

In light–matter interactions, the KH frame has played a decisive role for the development of an understanding of adiabatic stabilization [10]. We summarize here briefly the method of approach: assume for the moment that the Hamiltonian is perfectly periodic. Then from Floquet theory, a complete set of complex time-dependent eigenfunctions (quasi-stationary states) of the KH Hamiltonian can be constructed as follows:

$$\psi^{(\eta)}(r, \Omega, t) = \mathrm{e}^{-\mathrm{i}E^{(\eta)}t} \sum_{n=0}^{\infty} \phi_n^{(\eta)}(r, \Omega)\, \mathrm{e}^{-\mathrm{i}n\omega t} \tag{7}$$

where $E^{(\eta)}$ is the complex 'quasi-energy' of these states. Insertion of this expansion, together with a Fourier expansion of the time-dependent potential of equation (6),

$$V_a(r, \Omega, t) = V_{\mathrm{KH}} + \sum_{n\neq 0} V_n(r, \Omega)\, \mathrm{e}^{\mathrm{i}n\omega t}, \tag{8}$$

into the Schrödinger equation in the KH frame, leads to an infinite set of time-independent coupled differential equations for the components $\phi_n^{(\eta)}$ and the complex eigenvalues $E^{(\eta)}$,

$$\left(\frac{1}{2}\mathbf{p}^2 + V_{\mathrm{KH}} - (E^{(\eta)} + n\omega)\right)\phi_n^{(\eta)} = -\sum_{m\neq 0} V_m \phi_{m+n}^{(\eta)}. \tag{9}$$

The zero-order term V_{KH} represents the time average of the potential over a period, i.e.

$$V_{\mathrm{KH}} = \frac{1}{T}\int_T V_a(r, \Omega, t)\, \mathrm{d}t, \tag{10}$$

with T being the period of the laser. In the high-frequency limit ($\omega \to \infty$) the zero-order part of equation (9) dominates, and the set of Floquet equations reduces to one single [29],

$$\left(\tfrac{1}{2}\mathbf{p}^2 + V_{\mathrm{KH}} - E^{(\eta)}\right)\phi_0^{(\eta)} = 0, \tag{11}$$

with the formal solution

$$\psi^{(\eta)}(r, \Omega, t) = \mathrm{e}^{-\mathrm{i}E^{(\eta)}t}\phi_0^{(\eta)}(r, \Omega). \tag{12}$$

In this limit, the atom is completely stable against multiphoton ionization, i.e. for $\omega \to \infty$ the electron does not feel the rapid oscillations of the nucleus, but only its average value over a period. A *sufficient* criterion for stabilization is, $\omega \gg |W_0(E_0)|$, where $|W_0(E_0)|$ is the binding energy of the lowest eigenenergy state in the field. From this criterion, stabilization can occur when the external frequency is higher than internal (field free) frequencies of the electron. Adiabatic development from an initial field-free state to the ground state of V_{KH} when the field is on and back again is then possible. And in this very simple picture, the atom is completely stable against ionization. It was shown by Pont and Gavrila [30] that the ground state of the V_{KH} potential becomes less bound with increasing field strength. Hence, for a given frequency the stabilization process strengthens as the laser intensity increases.

From a modelling point of view, different physical processes are most efficiently described in different physical frames. In general, the description should start from a point which minimizes the perturbation and thus keeps the number of computational operations to a minimum. Thus, none of the equivalent descriptions of dipole limited light–atom interactions, equations (3), (5) and (6), is optimal for all kinds of laser frequencies, intensities and pulse durations. With $\mathbf{r}$ and $\mathbf{p}_l$ the conjugate variables describing position and momentum in the length gauge, the corresponding conjugate variables of the velocity gauge are $\mathbf{r}$ and $\mathbf{p}_v = \mathbf{p}_l - \mathbf{A}$. This may lead to fewer states required to describe the wavefunction in situations where $p_l \simeq A$, as has been shown in basis state expansions [26]. Unfortunately, however, the velocity gauge cannot be easily implemented in the numerical split step scheme below.

A comparison between the numerical properties of the velocity and length gauge with the KH frame has to the best of our knowledge not been carried out. By inspection however, the KH frame seems to be a natural frame for impulsive strong field processes, as strong field strengths will only reduce the magnitude of the Coulomb potential. Apart from regions in space where $\mathbf{r} \simeq \boldsymbol{\alpha}$, the KH frame thus minimizes the magnitude of the perturbation. The present scheme allows for direct implementation of both the length gauge and the KH frame Hamiltonians. In the following, we will compare the computational requirements necessary

to obtain frame invariance of the numerical results between the two Hamiltonians with the potentials in equations (5) and (6), respectively. The vector potential is here given by,

$$\mathbf{A}(t) = \frac{E_0}{\omega}\sin^2\left(\frac{t\pi}{T_{\text{pulse}}}\right)\sin(\omega t)\mathbf{u}_p. \tag{13}$$

This pulse ensures that the dc component of the field is zero. Furthermore, by keeping T_{pulse} an integer number n of laser cycles, $T_{\text{pulse}} = 2\pi n/\omega$, we are also guaranteed that the field displacement is zero at $t = T_{\text{pulse}}$. This makes a direct comparison of the wavefunction before and after the pulse possible without any additional transformations of the states [31].

In the simplest split step operator formulation, the wavefunction can be propagated from time t to $t + \Delta t$, with Δt small [32, 22] by,

$$\Phi(\mathbf{r}, t + \Delta t) \approx \mathrm{e}^{-\mathrm{i}\Delta t A/2}\,\mathrm{e}^{-\mathrm{i}\Delta t B/2}\,\mathrm{e}^{-\mathrm{i}\Delta t V_{l/a}(\mathbf{r},t)}\,\mathrm{e}^{-\mathrm{i}\Delta t B/2}\,\mathrm{e}^{-\mathrm{i}\Delta t A/2}\Phi(\mathbf{r}, t) \tag{14}$$

with $A = -\frac{1}{2}\frac{\partial^2}{\partial r^2}$ and $B = \frac{L^2(\Omega)}{2r^2}$. The overall numerical error per time step is here $\mathcal{O}(\Delta t^2)$. A common misunderstanding is to assume the global error of the scheme above to be $\mathcal{O}(\Delta t^3)$ which is the splitting error. This is however only true for time-independent Hamiltonians. For time-dependent Hamiltonians there is already a Δt^2 error in the time evolution operator defined by $\Psi(t_f) = T(t_f, t_0)\Psi(t_0)$, since,

$$T(t_f, t_0) = \mathrm{e}^{-\mathrm{i}(t_f - t_0)H} + \frac{\mathrm{i}}{2}\frac{\partial H}{\partial t}(t_f - t_0)^2 + \mathcal{O}(t_f - t_0)^3. \tag{15}$$

The second-order term is normally small for most laser processes. For short pulses towards attosecond duration, however, it is clear that this term is important and becomes the leading source of error.

Following Hansen *et al* [23], the trick is now to expand the wavefunction in orthonormal polynomials which is partly diagonal in A and B. By expanding in spherical harmonics,

$$\Phi(r_i, \Omega_{jk}, t) = \sum_{l=0}^{L_{\max}}\sum_{m=-l}^{l} f_{lm}(r_i, t)Y_{lm}(\Omega_{jk}), \tag{16}$$

we obtain,

$$f_{lm}(r_i, t) = \sum_{jk} w_{jk}Y^*_{lm}(\Omega_{jk})\Phi(r_i, \Omega_{jk}, t), \tag{17}$$

with abscissas and weights (Ω_{jk}, w_{jk}) recently published in tabular form [33]. The sum is truncated at $l = L_{\max}$, where $L_{\max}$ is chosen sufficiently large to assure convergence of the numerical scheme. The radial space is also truncated at $r_{\max}$ which is set large enough to cover the spatial extension of the wavefunction at all times during the pulse. With the present expansion the operator B simply reduces to a phase multiplication of each angular function by $\exp\left[\mathrm{i}\Delta t l(l+1)/4r_i^2\right]$. The operator A is correspondingly calculated by expanding each radial basis function in its Fourier components which reduce to another set of multiplications accompanied by two fast Fourier transformations. Following the action of these operators the wavefunction Φ is calculated at each grid point and the exponential potential operator $\mathrm{e}^{-\mathrm{i}\Delta t V_{l/a}(r_i,\Omega_{jk},t)}$ can act by straightforward multiplication.

The present method is ideal for 'near spherical' problems which restrict the number of necessary radial basis functions and keeps $L_{\max}$ to a minimum. It also has some built-in numerical advances such as providing an efficient parallel code [34], and it can be applied to the length gauge as well as the KH frame without extra programming.

The post-processing work needed to produce physical quantities following a numerical algorithm should also be considered. In the present scheme, this work is minimized since the

projection onto field-free eigenstates is particularly simple. For ionization, for example, the hydrogenic free particle wavefunctions can be expanded in the spherical harmonics,

$$\phi_c(k, r, \Omega) = \sum_{l=0}^{\infty} \sum_{m=-l}^{l} \mathrm{i}^l \, \mathrm{e}^{\mathrm{i}\sigma_l} R_l(k, r) Y_{lm}(\Omega) Y^{\star}_{lm}(\Omega_k). \tag{18}$$

Here $k = \sqrt{2E}$ is the wavenumber of the wavefunction, Ω_k is the spherical angle of the outgoing wave and $R_l(k, r)$ is a real radial wavefunction. Furthermore, σ_l is the Coulomb phase required to satisfy the boundary condition as $r \to \infty$ and $\sigma_l = \arg\Gamma\left(l + 1 + \frac{i}{k}\right)$. For an infinitely large r-space, k is a continuous variable, while here the discrete k-spectrum is directly obtained from maximum box size of the simulation, $r_{\max}$. The radial free particle Coulomb waves, $K_l(k, r)$, are found by iterative solution of

$$\frac{1}{2}k^2 K_{k,l}(r) = \left(-\frac{\mathrm{d}^2}{\mathrm{d}r^2} + \frac{l(l+1)}{2r^2} - \frac{1}{r}\right) K_{k,l}(r) \tag{19}$$

with boundary values $K_{k,l}(0) = K_{k,l}(r_{\max}) = 0$ where $K_{k,l}(r) = r R_l(k, r)$. It is then a matter of computational power to find the Coulomb waves for all valid values of k_i up to a chosen $k_{\max}$, and all values of $l \leqslant L_{\max}$. We must ensure that $k_{\max}$ is sufficiently high so that the probability of ionization to higher energies than $E_{\max} = k^2_{\max}/2$ is negligible.

Having found the radial Coulomb waves the energy distribution of the ionized electron is given as

$$\frac{\mathrm{d}P_I(k_i)}{\mathrm{d}k} = \frac{1}{\Delta k_i} \sum_{l,m} \left| \int_0^{r_{\max}} K_{k_i,l}(r) f_{lm}(r) \, \mathrm{d}r \right|^2. \tag{20}$$

We then easily calculate the total ionization probability by taking the sum over all discrete values of $E(k_i) = k_i^2/2$. Furthermore, the angular ionization distribution is given by

$$\frac{\mathrm{d}P_I(\Omega)}{\mathrm{d}\Omega} = \sum_{k_i} \left| \sum_{l,m} (-\mathrm{i})^l \, \mathrm{e}^{-\mathrm{i}\sigma_l} Y_{lm}(\Omega_k) \int_0^{r_{\max}} K_{k_i,l}(r) f_{lm}(r) \, \mathrm{d}r \right|^2. \tag{21}$$

Thus, as long as $r_{\max}$ is chosen large enough all measurable quantities can be directly calculated by simple one-dimensional integrals involving the final wavefunction directly.

We now return to the question of which frame is the most efficient for short laser pulses. In figure 1, we show the highest populated l-value for calculations in the length gauge and the KH frame, respectively, for a 5-cycle pulse, cf equation (13), with increasing intensity (upper figure) and an N cycle pulse with fixed intensity (lower figure). By highest populated l is meant the l value in equation (16) which is such that the probability for populating any higher state is always smaller than 10^{-3} during the pulse. Thus, the highest populated l value gives a direct indication of the maximum l needed to obtain convergence. By comparison, it is clear that the KH frame outmatches completely the length gauge in computational power. Both as a function of intensity and as a function of pulse length with fixed intensity, we observe that the KH frame stabilizes at a small number $L_{\max} \simeq 10$ as a necessary upper limit for the expansion in equation (16). The length gauge on the other hand requires increasingly higher value of $L_{\max}$ with increasing number of optical cycles and/or increasing intensity, and it will thus rapidly become prohibitive for three-dimensional calculations.

The KH frame combined with a spherical expansion thus becomes very efficient for non-perturbative laser–atom or laser–molecule simulations. We therefore apply the KH frame to the calculations in the following section. We have also checked the results by performing some of the calculations in the length gauge, and frame invariance within 1% was obtained for all cases.

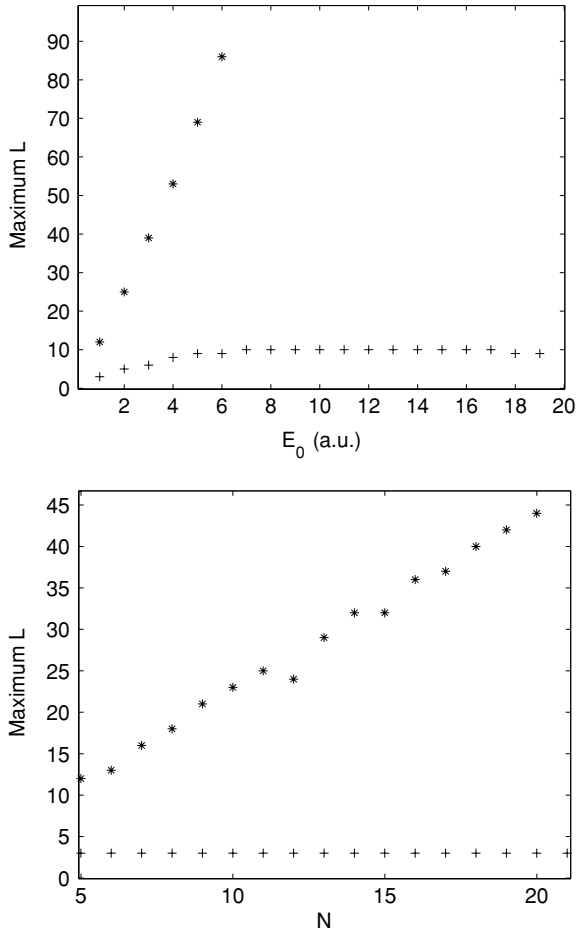

Figure 1. Upper: highest populated l as a function of field strength for a 5 cycle pulse with $\omega = 1.0$. Lower: highest populated l as a function of pulse length with $E_0 = 2.0$, and the pulse length is given by $T_{\text{pulse}} = N2\pi/\omega$. Both panels: '+' Kramers–Henneberger frame calculations; '$*$' Length-gauge calculations.

3. Results and discussion

We here report results from three-dimensional calculations of the ionization probabilities and characteristics of a H(2p) atom based on the outlined method of the previous section. The initial state is aligned along the z axis with magnetic quantum number $m = 0$, and exposed to a linearly polarized laser pulse defining an arbitrary angle with the initial quantization axis of the atom. The motivation behind the calculations is twofold; (i) to contribute to a more complete understanding of dynamical stabilization of excited atoms in intense laser fields and (ii) to investigate the geometrical aspects of ionization from aligned quantum states. As such, the latter point is related to ionization of aligned diatomic molecules as well as excited atomic states.

The calculations are carried out for 5-cycle pulses in the non-perturbative intensity regime. Two typical laser frequencies are applied, $\omega = 1.0$ (45 nm) and $\omega = 0.11$ (400 nm) which

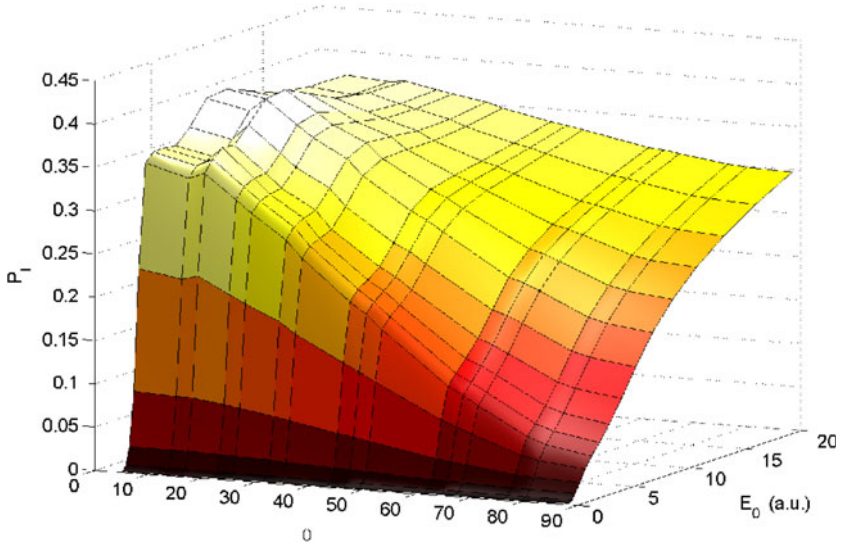

Figure 2. Ionization probability for 2p($m = 0$) hydrogen as a function of laser polarization θ and electric field strength E_0 for $\omega = 1.0$.

allow us to study the electronic response in a high frequency pulse of attosecond duration (760 as) versus the response to more conventional pulsed laser frequency in the femtosecond range (7 fs). The intensity ranges were set to $0 < E_0 < 20$ ($0 < I < 1.4 \times 10^{19}$ W cm^{-2}) and $0 < E_0 < 0.1$ ($0 < I < 3.4 \times 10^{14}$ W cm^{-2}) for the high and low frequency pulse, respectively. Other parameters of the calculations are, $L_{\max} = 12, r_{\max} = 300, 1024$ radial grid points and the time step $\Delta t = 0.01$. An absorbing boundary was used to remove unphysical high-frequency components. These components of the wavefunction carry initially a very small amplitude such that they do not destroy norm conservation significantly when damped at first contact with the boundary. The extension of the grid was always kept large enough to assure that the norm of the wavefunction remains very close to unity at the end of the pulse.

In figure 2, the ionization probability following a 5-cycle pulse with $\omega = 1.0$ is shown as function of the electric field intensity and the angle between the H(2p) symmetry axis and the polarization vector of the electric field, cf equation (13). The ionization probability is seen to depend critically on the angle θ for field strengths $1 < E_0 < 10$ with favoured ionization at small angles. At $E_0 = 1$ for example, the ionization probability is around ten times larger for $\theta \simeq 0$ compared to $\theta \simeq 90^\circ$. From a simple classical picture of an initial oscillating charge it seems reasonable with preferred orientation for $\theta = 0$, even if the laser frequency is much larger than the natural frequency of the electron, a phenomenon well known from fast ion–atom collisions [35]. In both cases, ionization is enhanced for minimum momentum transfer which is initially present in the parallel case. Another interesting aspect of figure 2 is that dynamic stabilization is most pronounced at small angles. Here the ionization probability reaches a maximum around $E_0 = 10$ and from there on decreases with increasing intensity. For larger values of θ, however, the ionization probability always increases with field intensity.

In figure 3, the ionization probability for a corresponding 5-cycle pulse with $\omega = 0.11$ is shown as function of field intensity in a comparable intensity region with respect to ionization probability. For this frequency we observe a much smaller angular ionization dependence,

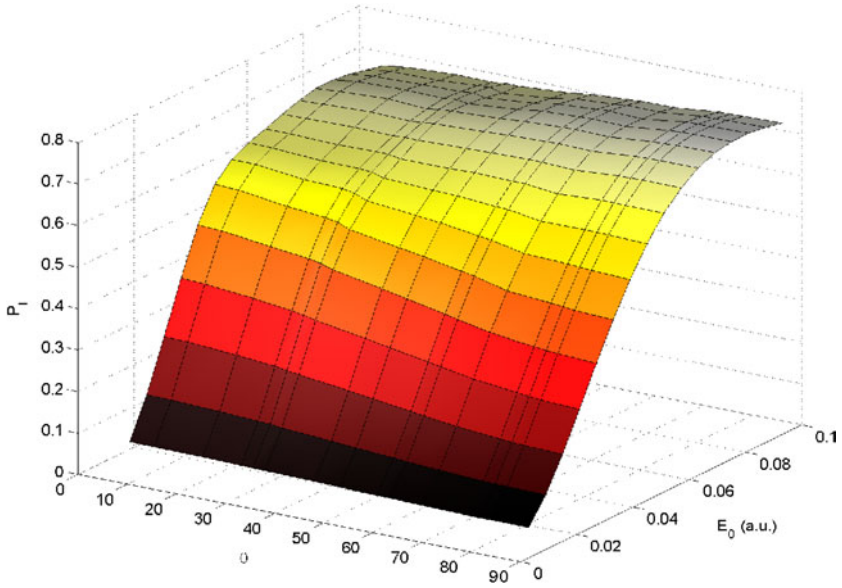

Figure 3. Ionization probability for 2p($m = 0$) hydrogen as a function of laser polarization θ and electric field strength E_0 for $\omega = 0.11$.

only about 30–40% in favour of small θ-values around $E_0 \simeq 0.02$. For high intensities, the ionization probability is completely independent of θ and the ionization probability stabilizes around 70%.

In figure 4, snapshots of the time development of the probability density are compared at corresponding times for the two pulses, i.e. after 1, 2 and 4 cycles. The left side shows $\omega = 0.11$ and polarization angle $\theta = 55^\circ$. We observe that the wavefunction has instantly responded to the laser polarization direction which results in a distinct radiative pattern. The right side of figure 4 shows snapshots for $\omega = 1.0$ and polarization angle $\theta = 90^\circ$. Here we observe that it does take several cycles for the oscillating field to release the electron.

The results in figures 2 and 3 are now interpreted by taking advantage of symmetry properties of the real spherical harmonics,

$$\begin{aligned} \widetilde{Y}_{l0} &= Y_{l0} \\ \widetilde{Y}_{lm} &= \tfrac{1}{\sqrt{2}}(Y_{lm} + (-1)^m Y_{l-m}) \qquad (m > 0) \end{aligned} \tag{22}$$

$$\widetilde{Y}_{l-m} = \tfrac{1}{\sqrt{2}}(Y_{lm} + (-1)^{m+1} Y_{l-m}) \qquad (m < 0). \tag{23}$$

When the electric polarization vector defines the quantization axis the initial wavefunction can thus be decomposed into two decoupled components,

$$\Phi(r, \Omega, t = 0) = [\cos\theta \widetilde{Y}_{10}(\Omega) + \sin\theta \widetilde{Y}_{11}(\Omega)] R_{21}(r, t = 0), \tag{24}$$

where $R_{nl}(r)$ is the hydrogenic radial wavefunction. The two components evolve independently, such that the wavefunction at a later time t can be written as

$$\Phi(r, \Omega, t) = \cos\theta \sum_{l=0}^{\infty} f_{l0}(r, t) \widetilde{Y}_{l0}(\Omega) + \sin\theta \sum_{l=1}^{\infty} f_{l1}(r, t) \widetilde{Y}_{l1}(\Omega). \tag{25}$$

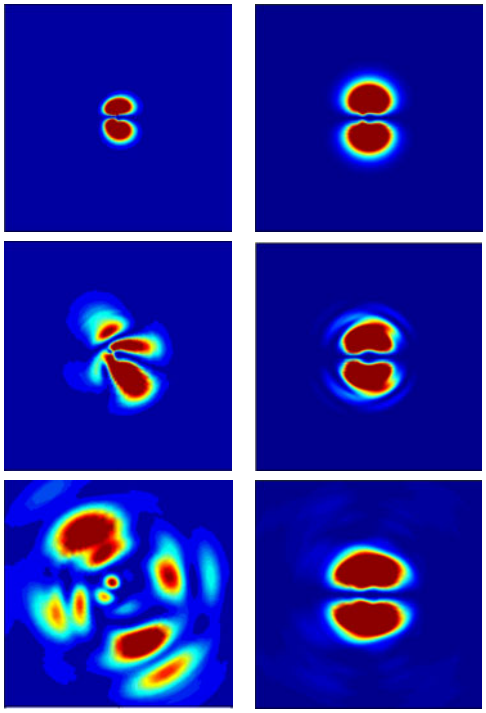

Figure 4. Snapshots of the probability density in the x–z plane at three different times during the laser pulse. Left: $\omega = 0.11$ and polarization angle $\theta = 55^\circ$. Right: $\omega = 1.0$ and polarization angle $\theta = 90^\circ$. Upper: snapshot after 1 cycle. Middle: after 2 cycles. Bottom: after 4 cycles. The scale at the left (right) panel is $\pm 50(\pm 30)$ in both directions.

The ionization probability may thus be expressed as

$$P_I(\theta, E_0) = p_0(E_0)\cos^2\theta + p_1(E_0)\sin^2\theta \tag{26}$$

with p_0 and p_1 being the corresponding ionization probabilities of the states $|2\mathrm{p}(m=0)\rangle_{\vec{u}_\mathrm{p}}$ and $|2p(m=1)\rangle_{\vec{u}_\mathrm{p}}$, defined with respect to the polarization direction of the field.

Now turning back to figure 2, equation (25) shows that the 1s state is symmetry forbidden when $\theta = 90^\circ$ for a linearly polarized field, whereas its importance for the dynamics is proportional to $\cos^2\theta$ as the angle θ is decreased. Hence, the stabilization dynamics will strongly depend on the relative population on the $|2\mathrm{p}(m=0)\rangle_{\vec{u}_\mathrm{p}}$ and $|2\mathrm{p}(m=1)\rangle_{\vec{u}_\mathrm{p}}$ states initially. For a given frequency, the $2\mathrm{p}(m=1)$ state stabilizes at a lower intensity than the $2\mathrm{p}(m=0)$ state. This is because the criterion for stabilization is fulfilled at lower intensities as long as the ground state in the field (1s state) is not populated during the period of the laser pulse. Similar considerations were made and exploited experimentally when atomic stabilization was first demonstrated in excited circular Rydberg states [36, 37]. These aspects explain the geometric variation of the ionization probability in figure 2. In fact, for $\theta \sim 90^\circ$ the frequency is already so high compared to the binding energy of the lowest accessible eigenenergy state in the field that multiphoton ionization is strongly suppressed at all intensities, whereas for $\theta \sim 0^\circ$ multiphoton processes occur for the lower field intensities. For the highest field strengths the effective binding energy ultimately becomes so low, independent of the polarization angle, that any dependence on θ vanishes.

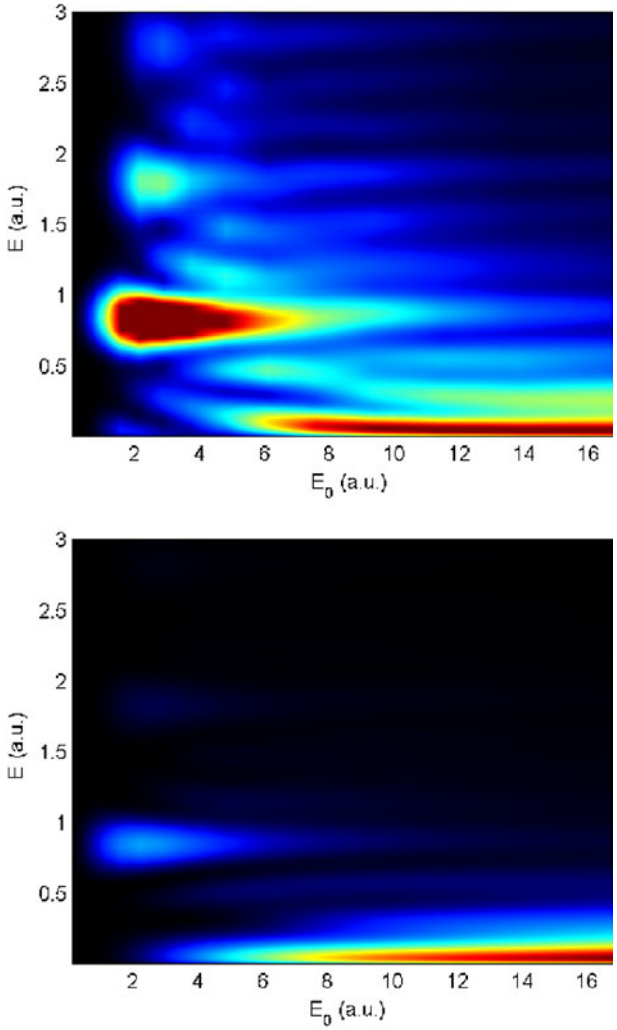

Figure 5. Upper: ionization probability density $\mathrm{d}P(E)/\mathrm{d}k$ as a function of electric field strength E_0 and energy of the ionized electron $E = k^2/2$ for $\omega = 1.0$. The polarization angle is constant at $\theta = 5^\circ$. Lower: same as upper, but $\theta = 88^\circ$.

Figure 5 shows the ionization probability density $\mathrm{d}P(E)/\mathrm{d}k$ versus electric field strength E_0 and energy E of the ionized electrons for $\omega = 1.0$, and for $\theta = 5^\circ$ and $\theta = 88^\circ$. A regular pattern of resonances corresponding to absorption of 1ω, 2ω and 3ω from the field is present at lower intensities for the lower angle, whereas only a weak signature of the one-photon resonance is visible for orthogonal polarization. The smaller peaks/resonances in the probability density appearing between the main resonances in the figure cannot be attributed to multiples of ω, but rather fractions of ω. They are a result of the non-adiabatic turn-on/-off of the field and are especially prominent for short pulses, and can be expected to be rather independent of the detailed pulse shape [38]. All essential features from the above discussion concerning directional dependences on the stabilization are confirmed, i.e. multiphoton ionization is strongly suppressed as $\theta \to 90^\circ$, whereas it is contributing significantly for smaller angles for $E_0 < 10$. Another important feature of figure 5 is the

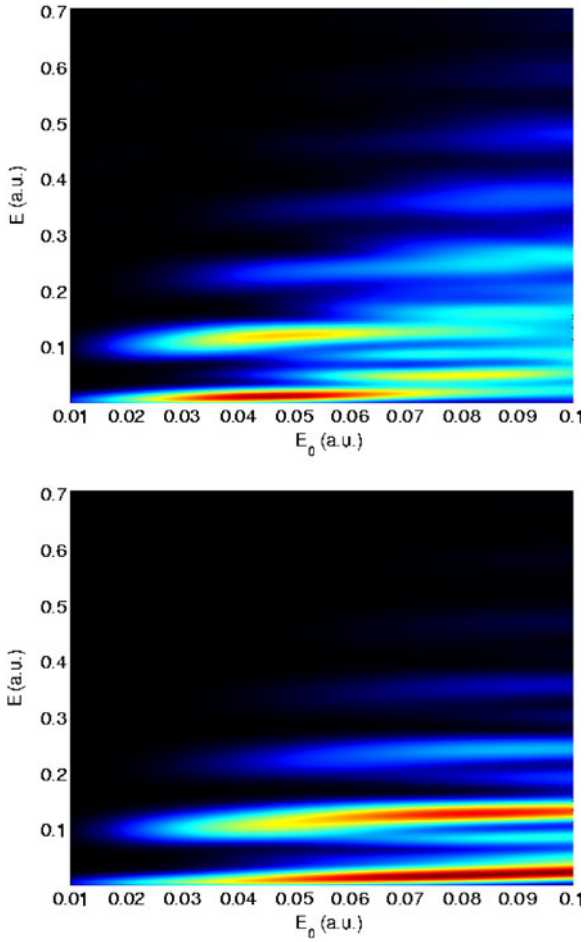

Figure 6. Ionization probability density $\mathrm{d}P(E)/\mathrm{d}k$ as a function of electric field strength E_0 and energy of the ionized electron $E = k^2/2$ for $\omega = 0.11$. The polarization angle is constant at $\theta = 5^\circ$. Lower: same as upper, but $\theta = 88^\circ$.

characteristic energies of the released electrons at high field intensities. The signatures of integral number of photon absorption vanish leaving only low energy electrons.

Referring to figure 3, for the lower frequency, $\omega = 0.11$, the geometric effect on the ionization is less pronounced, but still the trend is the same as for $\omega = 1.0$. A possible explanation for the much weaker orientation dependence is that the frequency (and/or intensity) of the laser is too low to support significant stabilization, independent of the polarization of the field. Furthermore, we suggest that the remaining dominating process, multiphoton ionization, only depends weakly on θ. The hypothesis is strengthened by comparison with figure 6, where $\mathrm{d}P(E)/\mathrm{d}k$ versus the electric field amplitude E_0 and energy E is shown for $\omega = 0.11$. Here multiphoton ionization processes are the dominating feature for all angles. The two spectra in figure 6 are similar, showing that the geometric effects are less important for ATI processes.

We now turn to the question whether the different θ behaviour gives rise to correspondingly different angular distributions of the ionizing electrons. Returning to equation (25) we can

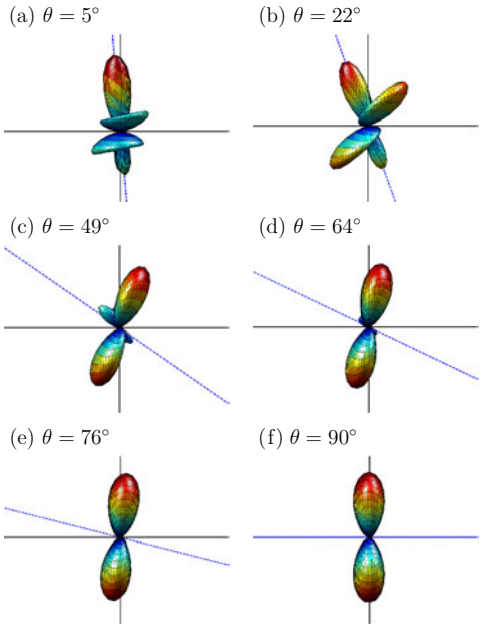

Figure 7. Angular ionization distribution, $\mathrm{d}P_I(\Omega)/\mathrm{d}\Omega$, for $\omega = 1$ and $E_0 = 9.3$ plotted in the x–z plane. The (blue) dashed line is the laser polarization direction θ. The snapshots of figure 4 result in the emission spectrum (f) of this figure.

express the differential cross section as

$$\frac{\mathrm{d}P_I(\Omega)}{\mathrm{d}\Omega} = \sum_{k_i} \left| \sum_l (-\mathrm{i})^l \, \mathrm{e}^{-\mathrm{i}\sigma_l} \left(a_{k_i,l} \cos\theta \widetilde{Y}_{l0}(\Omega_k) + a_{k_i,l} \sin\theta \widetilde{Y}_{l1}(\Omega_k) \right) \right|^2 \qquad (27)$$

with $a_{l,k_i} = \int_0^{r_{\max}} K_{k_i,l}(r) f_{l0}(r)\,\mathrm{d}r$ and $b_{l,k_i} = \int_0^{r_{\max}} K_{k_i,l}(r) f_{l1}(r)\,\mathrm{d}r$. In general several angular momentum states are populated in the final state so further simplification cannot be easily performed. In figures 7 ($\omega = 1.0$) and 8 ($\omega = 0.11$), the angular electron spectrum is plotted for a series of θ-values in the field intensity region where the angle dependence is most significant. In figure 7 we observe some interesting structures in the angular spectrum at small θ-values. This is caused by strong population and mixing of $l = 1, 2, 3$ states. At large θ-values multiphoton ionization is suppressed and only $l = 1$ remains significantly populated. From equation (27), we obtain a spectrum dominated by the $\widetilde{Y}_{11}$ term, which is indeed seen in the lower parts of figure 7.

The electron spectrum for $\omega = 0.11$ is completely different and dominated by the $l = 2$ component for all angles. At small angles, the azimuthal quantum number $m = 0$ determines the spectrum and at large angles $m = \pm 1$ appears on an equal footing giving rise to the four-leaf clover shape. At intermediate angles, we observe the up-building of a 'slippage angle' between the major electron emission direction and the laser polarization vector. This slippage mechanism is also well known as rotational (or Coriolis) coupling from ion–atom collisions [39].

When comparing the two frequencies in figures 5, 7 with figures 6, 8, it is clear that ionization by high frequency pulses results in completely different characteristics than conventional laser frequencies: $\Delta l = 0$ transitions dominate at high intensities resulting in angular spectra less sensitive to the laser polarization direction. The released electrons have

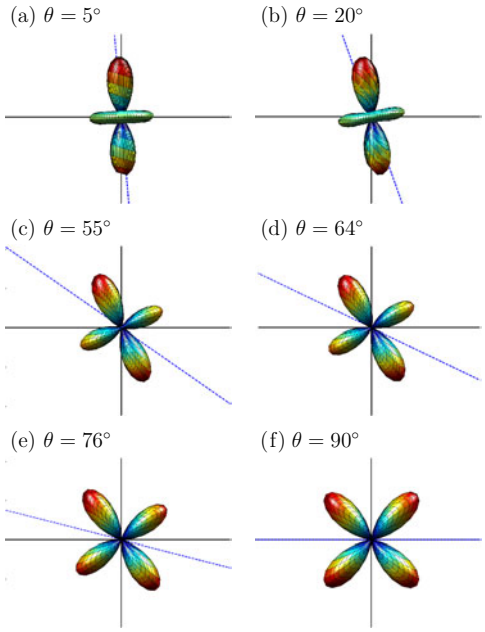

Figure 8. Angular ionization distribution, $\mathrm{d}P_l(\Omega)/\mathrm{d}\Omega$, for $\omega = 0.11$ and $E_0 = 0.04$ plotted in the x–z plane. The (blue) dashed line is the laser polarization direction θ. The snapshots of figure 4 result in the emission spectrum (c) of this figure.

an expected energy much lower than the energy corresponding to the central one-photon frequency.

4. Concluding remarks

The ionization dynamics of an initially aligned H(2p) atom exposed to angle-specified linear polarized 5-cycle laser pulses with central frequencies in the XUV ($\omega = 1.0$) and UV ($\omega = 0.11$) regimes has been analysed in detail. The analysis is based on results from a fully non-perturbative solution of the time-dependent Schrödinger equation in the Kramers–Henneberger frame on a spherical grid. The results have been interpreted on the basis of symmetry resolved basis functions.

Strong orientation effects in total ionization probability as well as differential probabilities in ejection angles and energy have been found in the XUV regime. The ionization probability at moderate intensities is ten times larger for the parallel polarization vector, $\theta = 0°$, than for perpendicular, $\theta = 90°$. Dynamic stabilization is found to be most pronounced at high frequencies and for polarization vectors parallel to the initial 2p state. At high intensities, multiphoton ionization vanishes resulting in the release of slow electrons propagating in a direction mostly determined by the initial charge cloud direction. For UV light, the effect of total orientation dependence is much more modest where the well-known $\Delta l = 1$ transition dominates the angular spectrum.

The geometrical results of this work are relevant for ongoing studies of ionization by aligned molecules [25] as well as the general understanding of atomic response to strong light sources of attosecond range duration. With rapid development of new intense laser sources,

an experiment measuring the kinetic electron spectrum from atoms can be directly compared with the present results.

Acknowledgments

The present research has been sponsored by Norges Forskningsråd through the Nanomat and Notur programmes.

References

[1] Baltuška A *et al* 2003 *Nature* **421** 611
[2] Drescher M *et al* 2002 *Nature* **419** 803
[3] Milosevic N, Corkum P B and Brabec T 2004 *Phys. Rev. Lett.* **92** 013002
[4] Peronne E, Poulsen M D, Bisgaard C Z, Stapelfeldt H and Seideman T 2003 *Phys. Rev. Lett.* **91** 043003
[5] Weber Th *et al* 2001 *Phys. Rev. Lett.* **86** 224
[6] Moshammer R *et al* 2000 *Phys. Rev. Lett.* **84** 447
[7] Makris M G and Lambropoulos P 2004 *J. Phys. B: At. Mol. Opt. Phys.* **37** 2247
[8] Lambropoulos P, Maragakis P and Zhang J 1998 *Phys. Rep.* **305** 1
[9] Eberly J H, Javanainen J and Rzazewski K 1991 *Phys. Rep.* **204** 331
[10] Gavrila M 2002 *J. Phys. B: At. Mol. Opt. Phys.* **35** R147
[11] Schafer K J, Gaarde M B, Heinrich A, Biegert J and Keller U 2004 *Phys. Rev. Lett.* **92** 023003
[12] Boca M, Muller H G and Gavrila M 2004 *J. Phys. B: At. Mol. Opt. Phys.* **37** 147
[13] Bauer D and Ceccherini F 2002 *Phys. Rev.* A **66** 053411
[14] Dundas D 2002 *Phys. Rev.* A **65** 023408
[15] Gajda M, Piraux B and Rzazewsky K 1994 *Phys. Rev.* A **50** 2528
[16] Andersen N, Gallagher J W and Hertel I V 1998 *Phys. Rep.* **165** 1
[17] Litvinyuk I V *et al* 2003 *Phys. Rev. Lett.* **90** 233003
[18] Zhao Z X, Tong X M and Lin C D 2003 *Phys. Rev.* A **67** 043404
[19] Kjeldsen T K, Bisgaard C Z, Madsen L B and Stapelfeldt H 2003 *Phys. Rev.* A **68** 063407
[20] Rotenberg B, Taieb R, Veniard V and Maquet A 2002 *J. Phys. B: At. Mol. Opt. Phys.* **35** L397
[21] Feuerstein B and Thumm U 2003 *Phys. Rev.* A **67** 063408
[22] Hermann M R and Fleck J A 1988 *Phys. Rev.* A **38** 6000
[23] Hansen J P, Sørevik T and Madsen L B 2003 *Phys. Rev.* A **68** 031401(R)
[24] Vázquez de Aldana J R and Roso L 1999 *Opt. Express* **5** 144
[25] Kjeldsen T K and Madsen L B 2004 *J. Phys. B: At. Mol. Opt. Phys.* **37** 2033
[26] Cormier E and Lambropoulos P 1996 *J. Phys. B: At. Mol. Opt. Phys.* **29** 1667
[27] Pauli W and Fierz M 1938 *Nuovo Cimento* **15** 167
Kramers H A 1956 *Collected Scientific Papers* (Amsterdam: North-Holland) p 866
Henneberger W C 1968 *Phys. Rev. Lett.* **21** 838
[28] Fritsch W and Lin CD 1991 *Phys. Rep.* **202** 1
[29] Gavrila M 1992 *Atoms in Intense Laser Fields* ed M Gavrila (San Diego: Academic) p 435
[30] Pont M and Gavrila M 1990 *Phys. Rev. Lett.* **65** 2362
[31] Madsen L B 2002 *Phys. Rev.* A **65** 053417
[32] Feit M D, Fleck J A and Steiger A 1982 *J. Comput. Phys.* **47** 412
[33] Sloan I H and Wommersley R S 2003 *Adv. Comput. Math.* http://www.maths.unsw.edu.au/rsw/Sphere/
[34] Hansen J P, Matthey T and Sørevik T 2003 A parallel split operator method for the time dependent Schrödinger equation *10th Euro PVM/MPI*
[35] Aumayr F, Gieler M, Schweinzer J, Winther H and Hansen J P 1992 *Phys. Rev. Lett.* **68** 3277
[36] de Boer M P, Hoogenraad J H, Vrijen R B, Constantinescu R C, Noordam L D and Muller H G 1993 *Phys. Rev. Lett.* **71** 3263
de Boer M P, Hoogenraad J H, Vrijen R B, Constantinescu R C, Noordam L D and Muller H G 1994 *Phys. Rev.* A **50** 4085
[37] van Druten N J, Constantinescu R C, Schins J M, Nieuwenhuize H and Muller H G 1997 *Phys. Rev.* A **55** 622
[38] Dondera M, Muller H G and Gavrila M 2002 *Phys. Rev.* A **65** 031405
[39] Kocbach L and Hansen J P 1990 *Phys. Scr.* **42** 317